19 Apr 2005

Bimetallic Pt-Ag and Pd-Ag Nanoparticles

Frank D. Blum
Missouri University of Science and Technology

Akira Tokuhiro
Missouri University of Science and Technology

Massimo F. Bertino
Missouri University of Science and Technology

Carmen M. Doudna

Bimetallic Pt–Ag and Pd–Ag nanoparticles

Debdutta Lahiri, Bruce Bunker,[a] and Bhoopesh Mishra
Department of Physics, University of Notre Dame, Notre Dame, Indiana 46556

Zhenyuan Zhang and Dan Meisel
Radiation Laboratory and Department of Chemistry and Biochemistry, University of Notre Dame, Notre Dame, Indiana 46556

C. M. Doudna, M. F. Bertino, Frank D. Blum, and A. T. Tokuhiro
Departments of Physics, Chemistry and Nuclear Engineering, University of Missouri–Rolla, Missouri 65409

Soma Chattopadhyay, Tomohiro Shibata, and Jeff Terry
Department of Biological, Chemical, and Physical Sciences (BCPS), Illinois Institute of Technology, Chicago, Illinois 60616

(Received 23 June 2004; accepted 17 February 2005; published online 19 April 2005)

We report studies of bimetallic nanoparticles with 15%–16% atomic crystal parameters size mismatch. The degree of alloying was probed in a 2-nm Pt core (smallest attainable core size) of Pt–Ag nanoparticles (completely immiscible in bulk) and 20-nm-diameter Pd–Ag nanowires (completely miscible in bulk). Particles were synthesized radiolytically, and depending on the initial parameters, they assume spherical or cylindrical (nanowire) morphologies. In all cases, the metals are seen to follow their bulk alloying characteristics. Pt and Ag segregate in both spherical and wire forms, which indicates that strain due to crystallographic mismatch overcomes the excess surface free energy in the small particles. The Pd–Ag nanowires alloy similar to previously reported spherical Pd–Ag particles of similar diameter and composition. © *2005 American Institute of Physics*. [DOI: 10.1063/1.1888043]

INTRODUCTION

There has been a great deal of interest in the size dependence of electronic and thermodynamic properties of metallic nanoparticles because of their potential use in many applications from catalysis to electronic devices. The electronic structure of a metallic nanoparticle undergoes major deviation from that of bulk.[1,2] Crystallographic parameters in these large clusters might be significantly different from those of the bulk, partially because of increased surface energy and partially because of capping agents that are always present when the particles are generated from suspensions in solution.[3] A significant impetus to study metallic nanoparticles comes from their ability to store excess electrons.[4] These stored electrons can reduce substrates in solution via multielectron-transfer processes, e.g., produce hydrogen from water. Bimetallic nanoparticles, composed of two different metal elements, are of greater interest since they offer a method to control the energy of the plasmon absorption band of the metallic mixture, which becomes a versatile tool in biosensing.[5] They may also improve the catalytic activity of the particles, sometimes creating new catalysts unknown in the bulk size.[6] Furthermore, structural changes can be created in small bimetallic nanoparticles as a result of alloying of the component metals, even though they remain segregated in bulk dimensions at ambient temperature. This may affect the electronic properties of the composite and may enhance or inhibit Fermi-level equilibration in such systems.[7]

Binary phase diagrams for bulk metals are a well-established, commonly utilized tool.[8] However, it is doubtful that they can be extended to the nanometer size regime because of the presence of the large bimetallic interface, the large surface area, and the possible presence of defects at the interface. A significant fraction of the total atoms present in the nanoparticles resides at the surface and contributes to the excess Gibbs free energy, thereby modifying the bulk binary phase diagram.[9,10] Similarly, a large fraction of the atoms occupies the bimetallic interface thereby affecting the miscibility of the metals in one another. Other factors that contribute to the modified alloying characteristics of the two metals are the depression of the melting point in clusters[11,12] and the presence of defects at the bimetallic interface of the particles that enhances the interdiffusion of the metals.[13] Both of these factors lead to an enhanced diffusion rate within the small particles, as much as nine orders of magnitude faster than in the bulk.[14] Size-dependent alloying in Au–Ag core-shell nanoparticles, at room temperature, had been reported by our group earlier.[13] At 2-nm Au core and variable thickness Ag shell, rapid random alloying has been observed at ambient temperature. However, for Au nanoparticles of $>$8-nm core size a distinct interface between the core and the Ag shell was maintained. In this context it should be noted that Au and Ag are bulk miscible at every ratio at elevated temperatures and they have essentially identical lattice parameters.

In the present report we explore the mixing behavior of Pt–Ag and Pd–Ag nanoparticles. In these systems the atomic sizes of the components differ by 15% and 16%, respectively, and the melting points of Pt and Pd are higher than that of the previously studied Au. In the bulk such a mis-

[a]Electronic mail: bunker.1@nd.edu

match results in a pronounced distortion of the alloy lattice and it might be expected that the solubility of one in the other will be difficult even in the nanoscale. It has been postulated that in order to obtain a primary solid solution the atomic radii should not differ by more than about 14%.[15] However, the large surface area, the increased surface free energy, and the reduced cohesive energy in the nanoparticles may partially relieve the mismatch-induced strain and increase the miscibility of the two metals. This competition between excess surface free energy and elastic relaxation has been analyzed in detail by Vanderbilt and co-workers.[16,17] Such theoretical studies have motivated us to explore such lattice-mismatched bimetallic systems.

To study the alloying of the two metals the x-ray-absorption fine structure (XAFS) technique was utilized.[18] The analysis is based on fitting the complex Fourier transform of the XAFS oscillations, revealing quantitative information about coordination numbers (N), bond lengths (r), and bond-length distribution (Debye–Waller factor) (σ^2) of the neighboring atoms. Unlike diffraction, XAFS does not require a high degree of crystallinity or long-range ordering in the sample to obtain high-quality data. Hence, the technique is particularly useful to extract structural information from disordered systems, such as powders or suspensions of nanoparticles. The part of the XAFS spectrum around the edge energy, called x-ray appearance near-edge structure (XANES), can be used to determine the oxidation state of the absorbing atom. A change in the oxidation state is reflected in a shift in the edge energy (from the pure metallic value) and "whiteline" features.[18] As mentioned above, we consider two systems, Pt–Ag and Pd–Ag; the bimetallic Pt–Ag is bulk immiscible, but it has been reported that deposition of Ag on Pt (111) leads to a monolayer-confined mixing.[19–21] The bimetallic Pd–Ag is bulk miscible[22] and it has already been shown that Pd–Ag spherical nanoparticles are miscible as well.[23] In the present report we examine cylindrical-shaped Pd–Ag nanoparticles (nanowires) to examine the effect of morphology on alloying. Both systems were synthesized using the radiolytic technique developed by Henglein and co-workers.[24] Using this technique and varying the experimental parameters allow morphology control of the particles. The size, shape, and composition of the samples were characterized by transmission electron microscopy (TEM) and a detailed analysis of the local structure was done using the XAFS technique. The XANES was observed to ensure that the samples did not oxidize during the measurements. The analysis leads to the conclusion that Pt and Ag do not alloy in the nanosize regime down to a diameter of 2 nm while Pd–Ag alloy even in the cylindrical rods.

EXPERIMENTAL SECTION

Materials and methods

Alloying of Au–Ag was observed at a core size of 2 nm;[13] hence we started at this small size for Pt core as well. The 2-nm Pt core particles were synthesized following Henglein *et al.*[24] A 70-ml solution containing 0.5-M methanol, 2×10^{-3} M sodium polyphosphate, 1×10^{-3} M sodium citrate, and 8×10^{-4} M K_2PtCl_4 (99.99%, Aldrich) was deaerated by bubbling Ar for 10 min and then irradiated in a ^{60}Co-γ source for 21 min at a dose rate of 9.6×10^2 krad/h. Irradiation was done in a 100-ml glass vessel that carried a sidearm cuvette made of high-purity quartz, so absorption spectra could be measured in complete isolation from air. After irradiation, 7-ml 0.2-M polyvinyl alcohol (PVA, M_w 50 000–85 000, Aldrich) was added to stabilize the Pt sol. Approximately 1 g of ion-exchange mixed-bed resin (Amberlite MB-150, Sigma) was added to decrease the concentration of free ions that remains from the various parent components and the solution was shaken overnight. The solution was separated from the resin, and 1.4-ml 0.1-M sodium citrate added to stabilize the Pt particles and the solution was filtered. This treatment with the ion-exchange resin was repeated and the absorption spectrum of the sol was measured after each treatment. The final concentration of Pt was about 5×10^{-4} M. All manipulations of the sol were carried out in a glove box under Ar atmosphere. The size of the roughly spherical Pt particles thus obtained was determined by TEM to be 2 ± 0.2 nm. The TEM image of these particles is shown in Fig. 1.

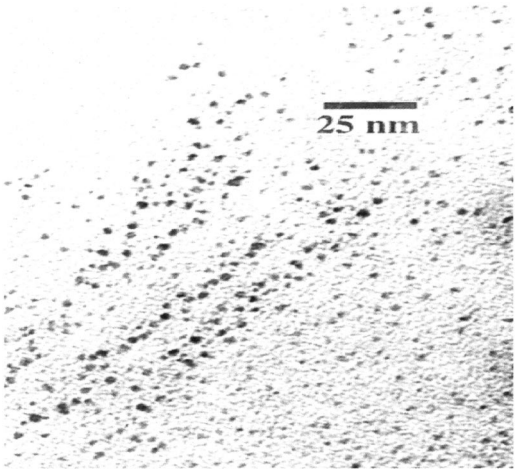

FIG. 1. TEM image of the 2-nm Pt nanoparticles. The particles were synthesized radiolytically and were used as core for the Pt–Ag particles.

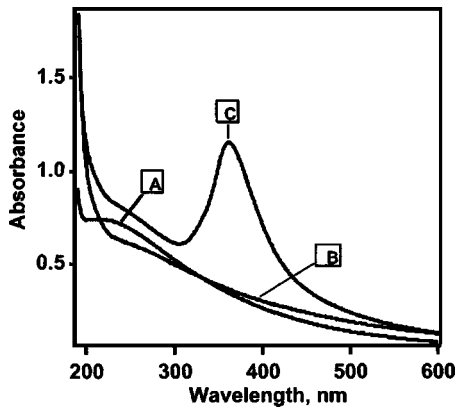

FIG. 2. UV spectra of 2-nm Pt (A) and 2-nm Pt particles coated with 1.2 (B) and 2.7 (C) layers of Ag. For A, $[Pt]=5\times10^{-4}$ M and its plasmon band is at 212 nm. For B, $[Pt]=3.3\times10^{-4}$ M, $[Ag]=3.3\times10^{-4}$ M, and $[Pt]/[Ag]=1:1$. For C, $[Pt]=2.5\times10^{-4}$ M, $[Pt]/[Ag]=1:3$, and its plasmon band is at 361 nm. Optical path is 2 mm.

TABLE I. Synthesis parameters for the formation of high-aspect ratio bimetallic nanoparticles.

PVA M_w (% hydrolysis)	Ag/Pt molar ratio	Ag and Pt compounds	Wire formation
31 000–170 000 (87–89)	80/20 to 20/80	H_2PtCl_6 and Ag_2SO_4	Yes
20 000 (98)	100/0, or 90/10, or 10/90, or0/100	K_2PtCl_4 and $AgNO_3$	No

To coat the Pt particles with a silver shell, the Pt sol was mixed with $AgClO_4$ and the mixture was bubbled with N_2O (in order to convert hydrated electrons produced in the forthcoming irradiation to OH radicals). Two samples of Pt:Ag concentration ratios of 1:1 and 1:3 were examined. These were irradiated in a ^{60}Co-γ source for 40 min (Pt:Ag=1:1, dose rate of 56.7 krad/h) and 60 min (Pt:Ag=1:3, dose rate of 2.04×10^2 krad/h). Complete reduction of Ag was confirmed when no change in the Ag plasmon band in the UV spectra could be observed following successive irradiations. The UV spectra of these samples are shown in Fig. 2. Assuming that the 2-nm Pt particles are roughly spherical and the Ag layers that are formed around the Pt core are fcc (111) surfaces, the number of Ag layers around Pt is calculated to be 1.2 and 2.7 for 1:1 and 1:3 ratios, respectively. Solid samples for XAFS measurements were prepared by allowing the suspensions to dry in the sample holder under inert atmosphere in a glove box.

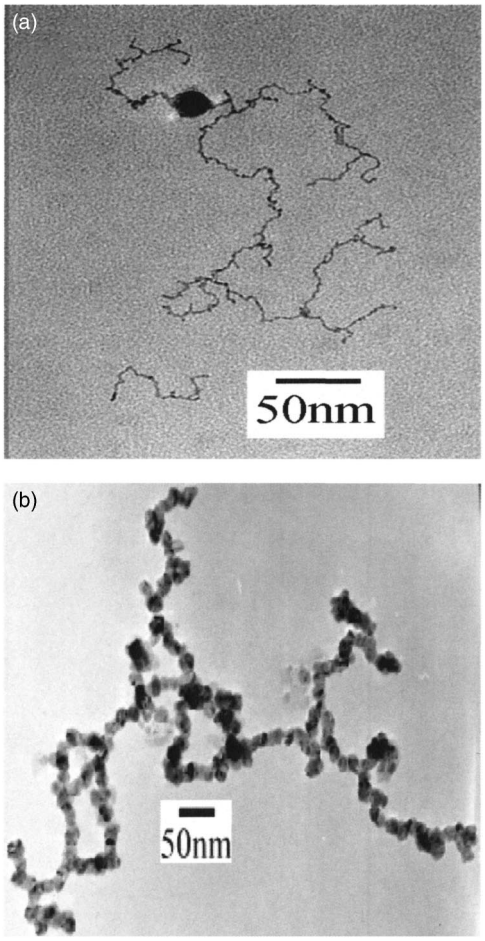

FIG. 3. Bright-field TEM micrographs of (a) Pt–Ag nanowires: A large particle of 20 nm and 85±5% Ag can be seen at the top of the figure. The thin filaments of 3-nm-diameter and 50% Ag extend out of the particle. (b) Pd–Ag nanowires: The wirelike particles have a diameter of 20–25 nm and a length of up to 1.5 μm.

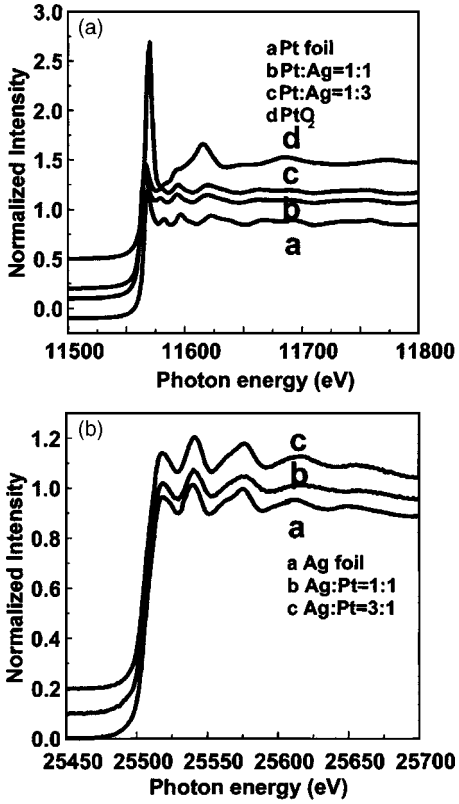

FIG. 4. XANES of Pt–Ag nanoparticles at (a) Pt L_3 edge and (b) Ag K edge. A comparison has been made with the respective foils. The XANES of the nanoparticles replicate the XANES of the pure metals and hence confirm that the samples have not been oxidized.

Pt–Ag nanorods were synthesized by radiolytic coreduction of salts of the two metals. Samples were prepared following the procedure of Doudna *et al.*[25] This approach is based on the observation that when a mixture of silver and

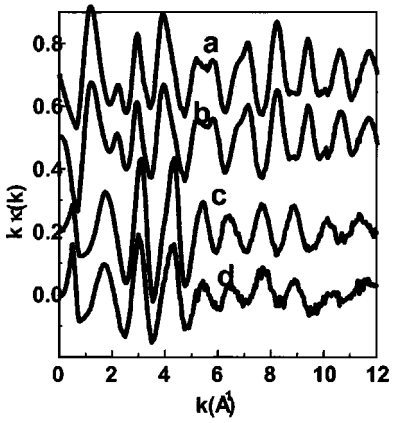

FIG. 5. The chi oscillations for the Pt–Ag nanoparticles with (a) Pt:Ag =1:3, at Pt edge (b) Pt:Ag=1:1, at Pt edge, (c) Pt:Ag=1:3, at Ag edge, and (d) Pt:Ag=1:1, at Ag edge. The data at Ag edge for the sample with Pt:Ag=1:1 look noisy because of the lower concentration of Ag in the sample. However, the quality was good enough to yield repeatable first shell near-neighbor features.

TABLE II. Fit parameters (coordination numbers) for Ag–Pt nanoparticles and standards.

Sample	*N* (Pt–Pt)	*N* (Pt–Ag)	*N* (Ag–Ag)
Pt foil	12±0.3	···	···
Pt nanoparticles	10.1±0.4	···	···
Pt:Ag 1:1 nanoparticles	10.0±0.1	1.32± 0.06	4.65±0.05
Pt:Ag 1:3 nanoparticles	9.8±0.2	1.31± 0.06	6.97±0.05

platinum salts is irradiated under reducing conditions, the former is reduced before the latter. The faster reduction of Ag^+ is due to the more positive reduction potential of Ag^+ relative to the multivalent platinum.[25] Under these circumstances, Ag seeds are initially formed and Pt shell is then deposited on them. Experimental conditions for rod-shape formation of these particles have been summarized previously and are outlined in Table I.[25] The rods are composed of two types of particles; large particles of typical diameters of 20–30 nm are joined by thin filaments of diameters of 2–5 nm. A TEM picture of the Ag–Pt nanowires is shown in Fig. 3(a). The elemental composition of the regions centered on the large particles and the filaments was determined using energy dispersive spectroscopy (EDS), with a spatial resolution of 150 nm. The large particles composed of 80%–90% Ag, while the filaments are close to 50% each, Ag and Pt. The EDS results suggest that the large Ag particles were formed in the early stages of the reduction, nucleation, and ripening while the Ag–Pt filaments result from the reduction of the Pt ions deposition on the Ag seeds. The Pd–Ag nanorods were synthesized similarly. Filamentlike particles, with typical diameters of 20–25 nm, and up to 1.5 μm long, were routinely observed after irradiation. The ratio between the two metals varied within the same particle and between nanoparticles, but the variation was, on average, within ±15% of the mole ratio of the original sample. The TEM picture of the Pd–Ag nanowires is shown in Fig. 3(b).

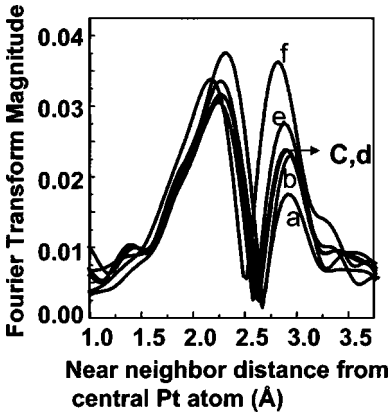

FIG. 6. EXAFS data at Pt edge for (a) 2-nm Pt core particle, (b) Pt foil and Pt core–Ag shell bimetallics of 2-nm core size with Pt:Ag ratios of (c) 1:3 and (d) 1:1. Simulations of a 2-nm Pt core with (e) Ag monolayer coating and (f) with Ag alloyed into the Pt core are also shown. The relative intensity of the peak at $r=3$ Å increases with an increased fraction of Ag near neighbors to Pt.

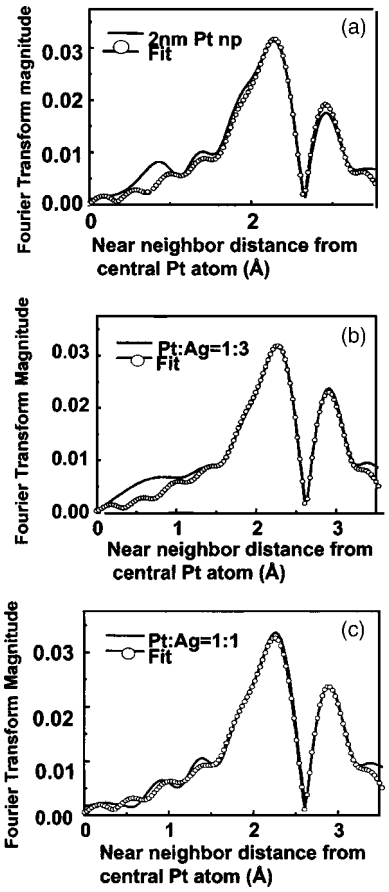

FIG. 7. Comparison of fit with the data at the Pt edge for samples with Pt:Ag ratio of (a) pure Pt nanoparticle (b) 1:3 and (c) 1:1.

The XAFS studies were performed at the MRCAT undulator beamline 10-ID at the Advanced Photon Source, Argonne National Laboratory. The measurements involved the Pt L_3 edge (11.564 keV), the Ag K edge (25.514 keV), and the Pd K edge (26.500 keV). The undulator parameters were optimized in the tapered mode to obtain a nearly constant intensity within the XAFS energy range. A cryogenic double-crystal Si (111) monochromator was utilized for x-ray energy selection. To eliminate unwanted higher harmonics from the monochromator, a Rh-coated harmonic rejection mirror at the Pt L_3 edge was used, while a Pt-coated mirror was used for the Pd and Ag K edges. The incident photon intensity was measured by an ion chamber filled with a mixture of 80% He and 20% N_2 gas at the Pt edge and 100% N_2 at Ag and Pd edges. At the Pt edge, x-ray fluorescence intensity was measured by a conventional three-grid "Lytle" ionization chamber detector filled with Kr gas. Since the concentration of Pt atoms in the sample was low, a thick Ga_2O_3 x-ray filter of nine absorption lengths was used to reduce background scattering and Soller slits were used to suppress multiple refluorescence from the filter. At the Ag and Pd edges, fluorescence flux was measured with the same Lytle detector with a six absorption-length Ru x-ray filter and Soller slits or, for some measurements, a 13-element Ge detector. For energy calibration, transmission-mode XAFS was measured on Pt, Ag, and Pd foils in parallel.

The extended x-ray-absorption fine structure (EXAFS) oscillations were isolated using standard methods. The edge

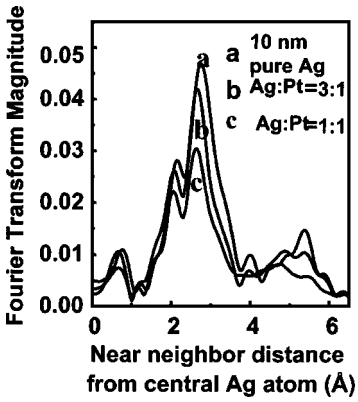

FIG. 8. EXAFS data at the Ag edge for (a) Ag nanoparticles of 10-nm size and Pt–Ag bimetallic nanoparticles with (b) 1:3 and (c) 1:1 Pt:Ag ratios. No Pt near neighbor was detected in these bimetallic nanoparticles.

energy, E', was determined by the point of inflection of the absorption spectrum. The preedge background was first subtracted from the raw data and normalized by the edge step. The postedge smooth background $[\chi_0(E)]$ was fitted to a polynomial to minimize the least-square deviation either using the AUTOBK program[26] or manually, and then subtracted from the normalized data $[\chi(E)]$. The oscillations were plotted as a function of the electron wave vector (k) using the relation $k=\sqrt{2m(E-E')/\hbar^2}$, where m is the electron mass and E' is the edge energy of the photoelectron. The $\chi(k)$ was then Fourier transformed into r space $[\chi(r)]$. A model was reasonably constructed and the theoretical scattering amplitudes and phase shift for this model are generated by FEFF (6.01a version). Structural parameters for the scattering were then determined using FEFFIT (Ref. 27) to give the best-fit values for bond lengths (r), coordination numbers (N), Debye–Waller factors σ^2 (and further degrees of disorder as necessary), and energy origin correction (E_0) arising from changes in the electronic energy levels by the presence of

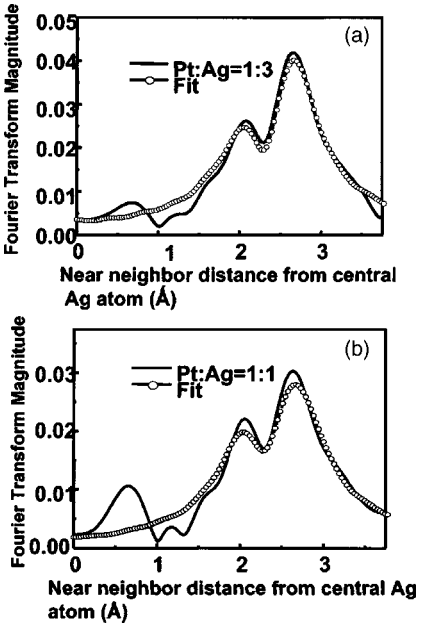

FIG. 9. Comparison of fit with the data at the Ag edge for samples with Pt:Ag ratios of (a) 1:3 and (b) 1:1.

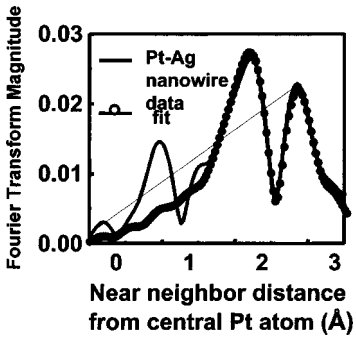

FIG. 10. EXAFS data at the Pt edge for the Pt–Ag bimetallic nanowire with 60% Pt are shown.

other atoms. The degree of alloying in bimetallic systems can be determined from the coordination number and/or the bond-length information. The fraction of near-neighbor coordination numbers for guest-guest and guest-host out of the total near-neighbor atoms can indicate the degree of alloying. Similarly, a systematic change of the interatomic distances in the host matrix, with the increased proportion of added guest-metal atoms, is considered to be a signature of alloying. Although the nearest-neighbor distances to each atomic species vary only slightly with alloy composition these changes can still be observed in the EXAFS parameters. On the other hand, if the two metals remain segregated, no significant change in the interatomic distances is observed.

RESULTS AND DISCUSSIONS

Pt–Ag system

The analysis is first done at the Pt L_3 edge and then at the Ag K edge. Prior to fitting, the XANES from the samples was observed to confirm that the metals were not oxidized. The XANES spectra at the Pt and Ag edges are shown in Figs. 4(a) and 4(b), respectively. The analysis at the Pt edge progresses in the following order:

(a) Pt foil fit;
(b) Pt nanoparticle fit. Approximating the seed Pt particles as spherical (from TEM) and comparing the fit results with those for the foil, determination of coordination loss due to surface effects;
(c) Pt–Ag determination of coordination number for the Pt:Ag=1:3 sample; and
(d) Pt–Ag determination of coordination number for the Pt:Ag=1:1 sample.

The XAFS oscillations from these samples are shown in Fig. 5. They were transformed in the k range of 3–11 $Å^{-1}$. Fit in r space was attempted between 1.4 and 3.2 Å for all the samples. The fit parameters are listed in Table II.

The decrease in the coordination number of Pt–Pt near neighbors in 2-nm Pt particles (10.06 ± 0.39) from that in Pt foil (12 ± 0.30) is due to coordination loss at the surface. Because of the large fraction of surface atoms, their contribution to the EXAFS results is as significant as that from the core atoms. Surface atoms constitute $\approx$53% of the total number of atoms for a 2-nm Pt particle with 10% size distribution, as indicated from TEM. From the measured coordina-

TABLE III. Fit parameters for Ag–Pd nanowires.

Sample name	Edge	Near-neighbor species	N	E_0 (eV)	r (Å^1)	σ (Å^2)
$Pd_{0.2}Ag_{0.8}$	Pd	Pd	9±1	−6.29±0.8	2.79±0.04	0.008±0.001
$Pd_{0.4}Ag_{0.6}$	Pd	Pd	9±5	−6.29 (fixed)	2.76±0.04	0.007±0.002
$Pd_{0.6}Ag_{0.4}$	Pd	Pd	9±6	−6.29 (fixed)	2.77±0.04	0.006±0.002
$Ag_{0.8}Pd_{0.2}$	Ag	Ag	10±1	3.55 (fixed)	2.83±0.02	0.008[a]
$Ag_{0.6}Pd_{0.4}$	Ag	Ag	9±1	3.55±0.2	2.80±0.04	0.007
$Ag_{0.4}Pd_{0.6}$	Ag	Ag	12±2	3.55 (fixed)	2.80±0.01	0.006

[a]Note that because the Ag and Pd distances are not resolved, both are approximated by a single distance and Debye–Waller factor.

tion number one estimates that for the Pt atoms at the surface approximately a third of the bonds are uncoordinated (3.7 dangling bonds).

To determine the degree of alloying in the 2-nm Pt core–Ag shell, the EXAFS spectra for complete coating of the Pt core with a layer of Ag were first simulated. Experimental results at the Pt edge for the two Pt:Ag ratios are compared with the simulations in Fourier-transformed r space in Fig. 6. The backscattering amplitude from Ag near neighbors, as well as the phase shift, differ from those of Pt. Correspondingly their Fourier transforms are different and the ratio of the peak heights at $r=2$ and $r=3$ Å depends on the ratio of Pt to Ag neighboring atoms. From the simulations in Fig. 4 one expects the intensity of the peak at $r=3$ Å to increase relative to that at $r=2$ Å with increasing the fraction of Ag near neighbors. From the experimental results of Fig. 5, it is clear that the number of Pt–Ag bonds in both samples is much lower than that suggested by the simulation of an alloyed mixture [Fig. 6(f) versus Figs. 6(c) and 6(d)] and is independent of the amount of Ag added. This implies that Ag does not alloy into the Pt core at ambient temperatures on this time scale but rather remain segregated.

For both the bimetallic samples, the fit results for the number of Pt–Pt bonds are seen to be equal to that for pure Pt nanoparticle within error limits (Table II). If alloyed, this number would have reduced from that of the pure particle since some of the Pt–Pt bonds would have been replaced by Pt–Ag bonds. Furthermore, fitting yields Pt–Ag coordination numbers of 1.32±0.06 for both the bimetallic samples. Comparing this Pt–Ag coordination number to Pt–Pt coordination number (10.06), one concludes that 1.32 out of the 3.7 available bonds, i.e., on the average, only 36% of the surface is covered with Ag in both the Pt–Ag core-shell samples, irrespective of the amount of Ag added. This indicates an eccentric growth of Pt and Ag nanoparticles. The Pt–Pt bond length in the bimetallic nanoparticles is found to be slightly smaller than that in bulk, viz., 2.73±0.01 Å (bulk value =2.75±0.004 Å), with a Debye–Waller factor $\sigma^2=0.004\pm0.001$ Å^2. The Pt–Ag bond length in the sample with Pt:Ag=1:3 is found to be 2.79±0.01 Å, with Debye–Waller factor $\sigma^2=0.006\pm0.001$ Å^2. The Pt–Ag bond length in the sample with Pt:Ag=1:1 is found to be 2.84±0.01 Å, with Debye–Waller factor $\sigma^2=0.006\pm0.001$ Å^2. A comparison of the fits with the respective data at the Pt edge for (a) a Pt nanoparticle of 2-nm size, (b) bimetallic particle with Pt:Ag=1:3, and (c) bimetallic particle with Pt:Ag=1:1 is shown in Fig. 7.

The XAFS oscillations at the Ag K edge are shown in Fig. 5. The data were transformed over the k range of 3–11 Å^{-1} and the fit was done in r space for the range of 1.0–3.75 Å and 1.0–3.68 Å for Pt:Ag ratios of 1:3 and 1:1, respectively. The parameters for the Pt–Ag bonds were fixed at the values obtained from the Pt L_3 edge for consistency. Results from the Ag K edge measurements on these bimetallic particles are shown and compared with pure Ag nanoparticles of 10-nm size in Fig. 8. The EXAFS of pure Ag nanoparticles of 10 nm resembles that of Ag foil, except for the slight coordination loss and a larger Debye–Waller factor. In the figure, we see that the bimetallic EXAFS merely replicates the pure Ag EXAFS. For alloying, one of the peaks should have increased more than the other.

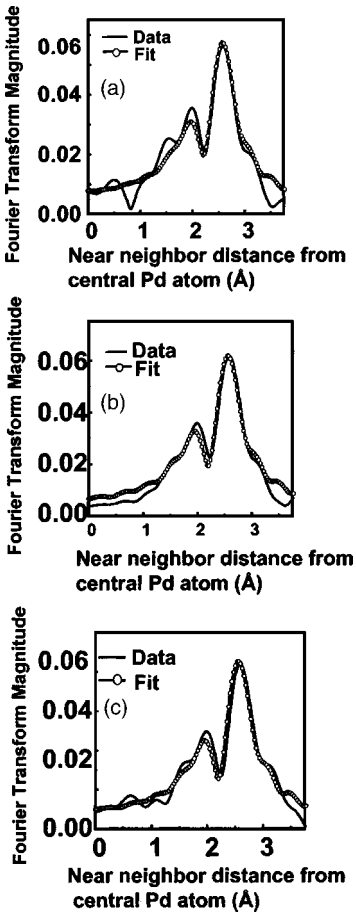

FIG. 11. Comparison of fit with the data at the Pd edge for (a) 20%, (b) 40%, and (c) 60% of Pd in the Pd–Ag nanowires.

The Ag–Ag coordination numbers in the Pt:Ag 1:3 and 1:1 samples are 6.97 ± 0.05 and 4.65 ± 0.05, respectively. This simply reflects the greater number of Ag atoms in the former case. This further confirms the observation from the Pt edge. Even with the addition of thrice the amount of Ag, the Ag atoms still tend to form an eccentric nanocluster rather than diffusing into the Pt core. To summarize, from both the Pt L_3 and Ag K edge data, it is concluded that Ag and Pt do not alloy at ambient temperature even in particles of 2-nm Pt core. Nearly complete alloying was reported for the Au–Ag system at a similar size and ambient temperatures. This difference is attributed to the different atomic size and lattice parameters for Pt–Ag system, which apparently require larger defect concentrations at the bimetallic interface for alloying to happen. Decreasing the core size may further induce alloying due to larger defects concentrations and higher diffusion coefficients induced by lower melting temperature. However, at present, we have been limited by synthesis difficulties and the smallest core size that could be reproducibly obtained was 2 nm. A comparison between the fits and the respective experimental data at the Ag K edge for (a) bimetallic with Pt:Ag=1:3 and (b) bimetallic with Pt:Ag=1:1 is shown in Fig. 9.

The structure of the Ag core–Pt shell nanowire was measured at the Pt L_3 edge. Experimental data and simulation for this nanowire at the Pt L_3 edge is shown in Fig. 10. The average Pt–Pt bond length in this bimetallic is found to be 2.74 ± 0.01, which is essentially the same as the interatomic distance in the bulk. Alloy formation would have led instead to an expansion of the average near-neighbor distance about Pt because of the larger atomic size of Ag. From this, it can be concluded that Pt and Ag do not alloy in the wire. The Pt–Ag coordination number is found to be (1 ± 0.2) and the Pt–Ag interatomic distance has been found to be 2.75 ± 0.05 Å, with a Debye–Waller factor of 0.006 ± 0.002 Å^2. Thus in all of the Ag–Pt samples, irrespective of their morphology, no significant signature of alloying is observed.

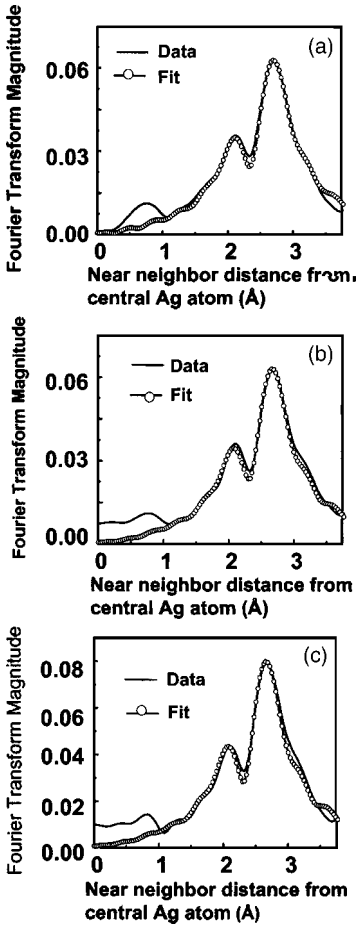

FIG. 12. Comparison of fit with the data at the Ag edge for (a) 20%, (b) 40%, and (c) 60% of Pd in the Pd–Ag nanowires.

Pd–Ag system

Pd and Ag are adjacent to one another in the Periodic Table. Therefore, their backscattering amplitude and phase effects on the photoelectron wave are nearly identical and it is very difficult to distinguish between these two near-neighbor species around the central atom. Fortunately, the near-neighbor distances of Pd and Ag are quite different, with the "natural" Pd–Pd bond length of 2.75 Å and the natural Ag–Ag bond length of 2.88 Å, as seen in the pure metals. With an increased fraction of the larger Ag atoms in the nanowires, both the average nearest-neighbor bond length around Pd and the Debye–Waller factor are expected to systematically increase.

Like the Pt–Ag nanoparticles, the Pd–Ag nanowires do not show any sign of oxidation. The data quality is of the same order as that for the Pt–Ag nanoparticles. We consid-

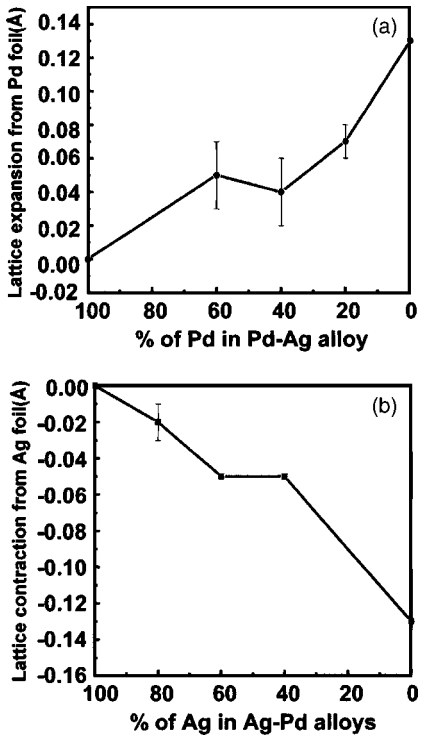

FIG. 13. (a) Bond-length expansion from the Pd edge for Pd–Ag bimetallic nanowires of several Pd:Ag ratios. The bond length systematically expands upon increasing Ag content. This indicates alloying. (b) Bond contraction from the data at the Ag edge for Pd–Ag bimetallic nanowires of several Pd:Ag ratios. The bond lengths in the bimetallic nanoparticles show a systematic contraction from Ag–Ag bond lengths upon increasing Pd content.

ered three different models for the neighbors around a central Pd atom: (a) Pd atoms only, (b) Ag atoms only, and (c) a mixture of Ag and Pd atoms. This is because, in spite of the similarity between scattering characteristics of Ag and Pd, the fit parameters were seen to vary slightly upon changing the near-neighbor species. This variation has been included in our estimate of errors. The fitting parameters for the average near-neighbor distances around Pd atoms and the Debye–Waller factors as determined at the Pd *K* edge are given in Table III as function of the mol % of Pd in the Pd–Ag sample. The errors in the parameters also include correlation between the various parameters. Despite the uncertainties, the change in the average near-neighbor distance, as a function of the mole fraction of the guest metal, is clearly systematic and significant. A comparison of the simulation with the experimental data at the Pd *K* edge is shown in Fig. 11, for various proportions of Pd in the alloys.

The conclusions from the results at the Pd *K* edge are corroborated by the results at the Ag edge. The fit parameters are listed in Table III. A comparison of the simulations with the experimental data at the Ag *K* edge is shown in Fig. 12, for the various proportions of Ag in the nanowires. The expansion in near-neighbor distance around Pd, as a function of increased proportion of Ag in the nanowires, is plotted in Fig. 13(a), and the contraction around Ag, as a function of increased proportion of Pd, is shown in Fig. 13(b). These systematic changes in the bond length indicate random alloying of Pd and Ag in these nanowires.

CONCLUSIONS

Pt and Ag (which are bulk immiscible) do not alloy even at a core size of 2 nm, although Ag and Au were seen to alloy at the same size. The separation between the two metals is maintained because of the strain induced in the Ag–Pt lattice as a result of lattice mismatch. The concentration of defects in such small particle size is not enough to initiate alloying. The segregation of Ag and Pt has also been observed in the cylindrical nanorods. On the other hand, Ag and Pd in nanowires (bulk miscible) are seen to alloy at room temperature, similar to their spherical counterparts. Thus the morphology of the nanostructure has little effect on its ability to alloy in these systems and at these dimensions.

ACKNOWLEDGMENTS

Work performed at MRCAT is supported in part by funding from the US Department of Energy under Grant No. DE-FG02-04ER46106. The work done at the Notre Dame Radiation Laboratory has been funded by the US Department of Energy under Contract No. 4568.

[1] R. Kubo, J. Phys. Colloq. **2**, C2-69 (1977).
[2] I. J. Friedel, Ann. Phys. (N.Y.) **1**, 257 (1976).
[3] R. L. Whetten, M. N. Shafigullin, J. T. Khoury, T. G. Schaaff, I. Vezmar, M. M. Alvarez, and A. Wilkinson, Acc. Chem. Res. **32**, 397 (1999).
[4] A. Henglein, Top. Curr. Chem. **143**, 113 (1988).
[5] J. M. Nam, C. S. Thaxton, and C. A. Mirkin, Science **301**, 1884 (2003).
[6] G. C. Bond and D. T. Thompson, Catal. Rev. - Sci. Eng. **41**, 319 (1999).
[7] A. Henglein, A. Holzwarth, and P. Mulvaney, J. Phys. Chem. **96**, 8700 (1992).
[8] W. G. Moffett, *The Handbook of Binary Phase Diagrams* (Genium Pub. Corp., Schenectady, NY, 1984).
[9] M. Wautelet, J. P. Dauchot, and M. Hecq, Nanotechnology **11**, 6 (2000).
[10] R. Vallee, M. Wautlet, J. P. Dauchot, and M. Hecq, Nanotechnology **12**, 68 (2001).
[11] H. Sakai, Surf. Sci. **351**, 285 (1996); Ph. Buffat and J-P. Borel, Phys. Rev. A **13**, 2287 (1976); C. L. Cleveland, W. D. Luedtke, and U. Landman, Phys. Rev. B **60**, 5065 (1999); K. K. Nanda, S. N. Sahu, and S. N. Behera, Phys. Rev. A **66**, 013208 (2002).
[12] K. Dick, T. Dhanasekaran, Z. Zhang, and D. Meisel, J. Am. Chem. Soc. **124**, 2312 (2002).
[13] T. Shibata, B. A. Bunker, Z. Zhang, D. Meisel, C. F. Vardeman, and J. D. Gezelter, J. Am. Chem. Soc. **124**, 11989 (2002); T. Shibata, H. Tostmann, B. A. Bunker, A. Henglein, D. Meisel, S. Cheong, and M. Boyanov, J. Synchrotron Radiat. **8**, 545 (2001).
[14] H. Yasuda, H. Mori, M. Komatsu, K. Takeda, and H. Fujita, J. Electron Microsc. **41**, 267 (1992); H. Mori, H. Yasuda, and T. Kamino, Philos. Mag. Lett. **69**, 279 (1994).
[15] W. Hume-Rothery, G. W. Mabbott, and K. M. Channel-Evans, Philos. Trans. R. Soc. London, Ser. A **233**, 1 (1934).
[16] D. Vanderbilt and L. K. Wickham, Mater. Res. Soc. Symp. Proc. **202**, 555 (1991).
[17] O. L. Alerhand, D. Vanderbilt, R. D. Meade, and J. D. Joannopoulos, Phys. Rev. Lett. **61**, 1973 (1988).
[18] *X-ray Absorption: Principles, Applications and Techniques of EXAFS, SEXAFS and XANES*, edited by D. C. Koningsberger and R. Prins (Wiley, New York, 1988).
[19] J. S. Tsay, Y. D. Yao, and C. S. Shern, Phys. Rev. B **58**, 3609 (1998).
[20] H. Röder, R. Schuster, H. Brune, and K. Kern, Phys. Rev. Lett. **71**, 2086 (1993); H. Röder, K. Bromann, H. Brune, and K. Kern, Surf. Sci. **376**, 13 (1997).
[21] A. F. Becker, G. Rosenfeld, B. Poelsema, and G. Comsa, Phys. Rev. Lett. **70**, 477 (1993).
[22] S. Müller and A. Zunger, Phys. Rev. Lett. **87**, 165502 (2001); A. Gonis, W. H. Butler, and G. M. Stocks, *ibid.* **50**, 1482 (1983); N. Takano, A. Yoshiwaka, and F. Terasaki, Solid State Commun. **107**, 213 (1998); I. Coulthard and T. K. Sham, Phys. Rev. Lett. **77**, 4824 (1996); K. H. Chae *et al.*, Phys. Rev. B **53**, 10328 (1996); G. Battaglin *et al.*, Nucl. Instrum. Methods Phys. Res. B **191**, 392 (2002); Y.-H. Chen, Y.-H. Tseng, and C.-S. Yeh, J. Mater. Chem. **12**, 1419 (2002); C. M. Doudna, M. F. Bertino, and A. Tokuhiro, Langmuir **18**, 2434 (2002).
[23] K. H. Chae *et al.*, Phys. Rev. B **53**, 10328 (1996).
[24] A. Henglein, B. G. Ershov, and M. Malow, J. Phys. Chem. **99**, 14129 (1995); A. Henglein and D. Meisel, Langmuir **14**, 7392 (1998).
[25] C. M. Doudna, M. F. Bertino, F. Blum, A. Tokuhiro, D. Lahiri-Dey, S. Chattopadhyay, B. A. Bunker, and J. Terry, J. Phys. Chem. B **107**, 2966 (2003).
[26] M. Newville, P. Livins, Y. Yacobi, E. A. Stern, and J. J. Rehr, Phys. Rev. B **47**, 14126 (1993).
[27] M. Newville, J. Synchrotron Radiat. **8**, 96 (2001); M. Newville, B. Ravel, D. Haskel, J. J. Rehr, E. A. Stern, and Y. Yacoby, Physica B **208–209**, 15 (1995).